Materials Science & Engineering A 615 (2014) 87–91

Contents lists available at ScienceDirect

Materials Science & Engineering A

journal homepage: www.elsevier.com/locate/msea

Depth dependent strain rate sensitivity and inverse indentation size effect of hardness in body-centered cubic nanocrystalline metals

J. Zhao [a], F. Wang [a,*], P. Huang [b,**], T.J. Lu [a], K.W. Xu [b]

[a] State Key Laboratory for Strength and Vibration of Mechanical Structures, School of Aerospace, Xian Jiaotong University, Xi'an 710049, People's Republic of China

[b] State Key Laboratory for Mechanical Behavior of Material, Xi'an Jiaotong University, Xi'an 710049, People's Republic of China

ARTICLE INFO

Article history:
Received 27 May 2014
Received in revised form
10 July 2014
Accepted 20 July 2014
Available online 29 July 2014

Keywords:
Indentation size effect
Strain rate sensitivity
Surface effect
Body-centered cubic

ABSTRACT

Size effects on hardness (H) and strain rate sensitivity (m) of nanocrystalline (NC) body-centered cubic Mo thin film were examined under nanoindentation testing. Contrast to existing reports that there was no indentation size effect on hardness in NC metals, inverse *indentation size effect* (ISE) in NC Mo was observed for the first time at penetration depths ranging from 15 to 200 nm, at all the loading strain rates applied. In addition, the strain rate sensitivity of NC Mo exhibited strong dependence on penetration depth, increasing dramatically with decreasing penetration depth. Surface effects related to two deformation mechanisms were proposed to be responsible for the observed inverse ISE on H and depth dependent m. Specifically, the mobility of screw dislocation/component and the diffusion length of interfacial diffusion were altered as the deformed region underneath the indenter was approaching the free surface, resulting in the unusual size effects in NC Mo.

1. Introduction

Indentation size effect (ISE), i.e., indentation hardness increasing with decreasing penetration depth, has been observed and well documented in the past two decades for a wide range of materials. Despite that ISE was considered in the earlier years as an artifact caused by either sample surface preparation or measurement error, both the Taylor dislocation model [1] and the model related to geometrically necessary dislocations within the deformed region [2] have been widely applied and accepted in interpreting specific size effect in indentation testing. However, ISE was only observed in single crystal and coarse grained metals and only few studies reported that nanocrystalline (NC) metals exhibit ISE during indentation [3]. The absence of ISE in fine-grained polycrystals (NC metals in particular) if the indentation size is comparable to or exceeds grain size is attributed to the fact that grain boundaries are strong barriers for dislocations [4], restricting the aforementioned two dislocation related models to operate in NC metals.

While significant efforts were devoted to characterizing ISE in face-centered cubic (fcc) metals, few concerned body-centered cubic (bcc) metals. Due to different dislocation mechanisms, the plastic deformation behavior of bcc metals is quite different from fcc metals. Unlike fcc metals, as a result of non-planar core structure and the associated high Peierls barrier, dislocation movement in bcc metals occurs on various slip systems and screw dislocations are slower than edge dislocations below critical temperature [5]. Moreover, it has been indicated that, opposite to trend observed in fcc metals, the strain rate sensitivity of bcc metals decreases with decreasing grain size [6]. The high strain rate sensitivity in coarse grained bcc metals was attributed to kink-pair assisted motions of screw dislocations. In contrast, the density of screw dislocations is quite low in NC bcc metals, results in their low strain rate sensitivity. In addition, Kaufmann et al. [7] indicated recently that surface effect could significantly enhance screw dislocation mobility in bcc metals, and surface effect may attribute to ISE significantly in a certain way [4]. Therefore, upon indentation testing, the penetration depth dependent hardness may be quite different from the ISE reported previously. This may therefore provide further insights to the physical mechanisms underlying the plastic deformation behavior of near-surface layers in crystalline metals.

In the present study, the penetration depth dependent hardness and strain rate sensitivity of NC Mo thin films were investigated by nanoindentation testing. Intriguingly, at all the loading strain rates applied in indentation hardness testing, inverse-ISE was observed and the strain rate sensitivity of hardness increased dramatically with decreasing penetration depth in the NC Mo. It was proposed that surface effects affecting the mobility of screw

* Corresponding author.
** Corresponding author.
E-mail addresses: wangfei@mail.xjtu.edu.cn (F. Wang), huangping@mail.xjtu.edu.cn (P. Huang).

http://dx.doi.org/10.1016/j.msea.2014.07.057
0921-5093/

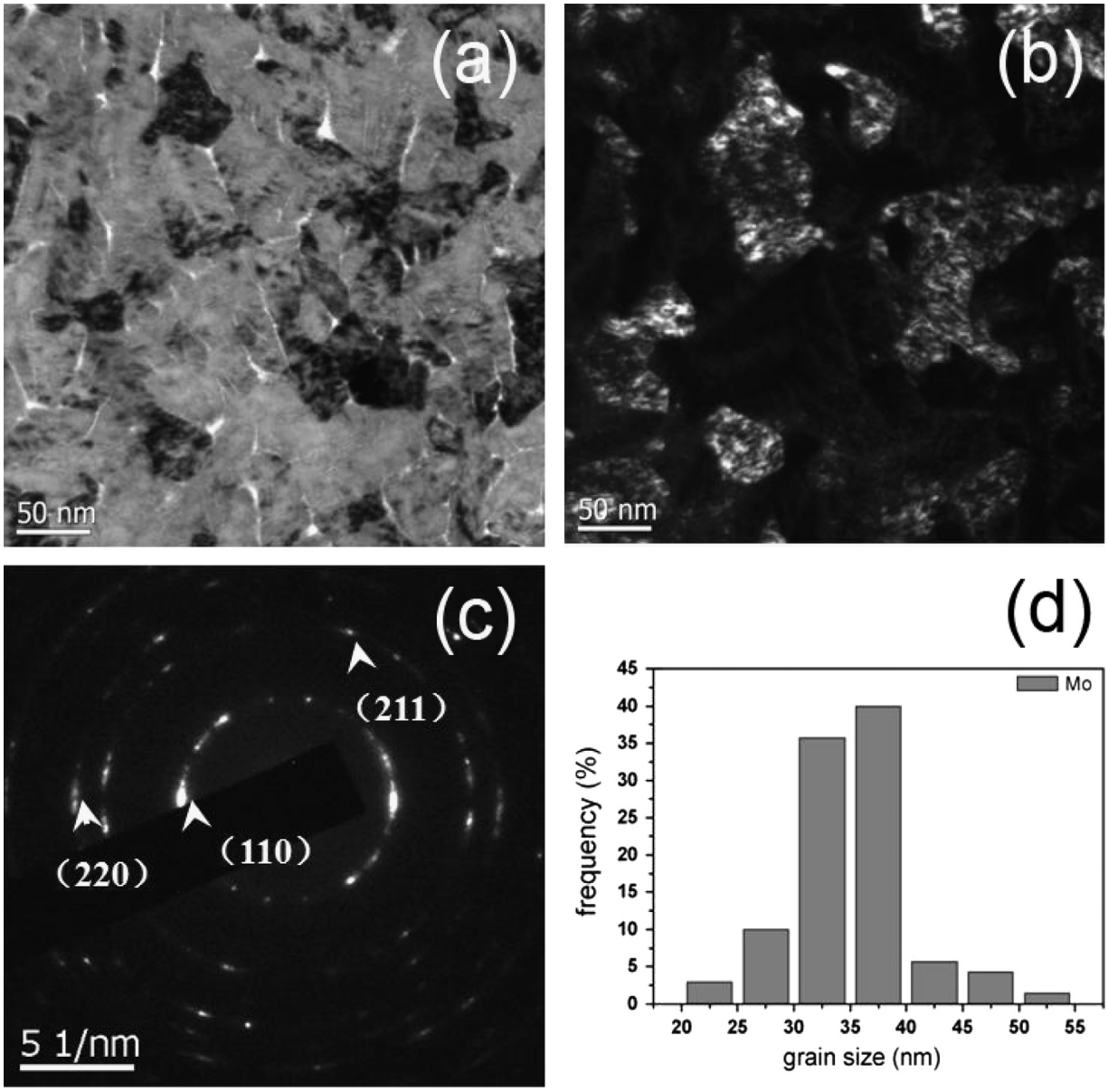

Fig. 1. . (a) Typical plan-view TEM bright-field image of NC Mo thin film; (b) corresponding dark-field image of (a); (c) electron diffraction (SAED) pattern of (a) and (b); (d) grain size distribution in NC Mo.

dislocation and the diffusion path along the indenter-specimen interface were the dominant mechanisms underlying the unusual size effects observed.

2. Experiments

2.1. Sample preparation and microstructure characterization

NC Mo thin film with thickness of 1350 nm was deposited via *d.c.* magnetron sputtering on a single silicon wafer (100) using a high purity target Mo (purity of 99.999%) under argon pressure of 0.3 Pa at room temperature. Transmission electron microscopy (TEM) and high resolution TEM (HRTEM) observations were carried out by using a JEOL 2100F microscope (Tokyo, Japan) under accelerating voltage of 200 kV.

Fig. 1(a) and (b) presented the plan-view bright-field and dark-field TEM micrographs of the Mo film, while Fig. 1(c) displayed the corresponding electron diffraction patterns. The average grain size of the Mo film was estimated to be about 34.8 nm, with relatively narrow grain size distribution.

Fig. 2 displayed the HRTEM images of the lattice structure within a typical grain in the Mo film, in which the corresponding zone axis is [001]. As shown in the magnified figure of Fig. 2(b), four dislocations could be identified, i.e., full dislocations of $1/2[\bar{1}\,\bar{1}1]$(h, n) and $1/2[11\bar{1}]$(k, m). Clearly, the Burgers vectors were neither parallel nor perpendicular to the dislocations. Therefore, the observed four dislocations in Fig. 2 were all mixed dislocations having both edge and screw components. In addition, the density of dislocations in the grain shown in Fig. 2(b) was estimated to be about $\sim 10^{16}\ m^{-2}$.

2.2. Nanoindentation testing

Nanoindentation tests were performed on MTS Nanoindenter XP system (MTS, Inc) under Continuous Stiffness Measurement (CSM) mode at ambient temperature, with the applied loading strain rate (LSR) ranging from $0.005\ s^{-1}$ to $0.2\ s^{-1}$. After the

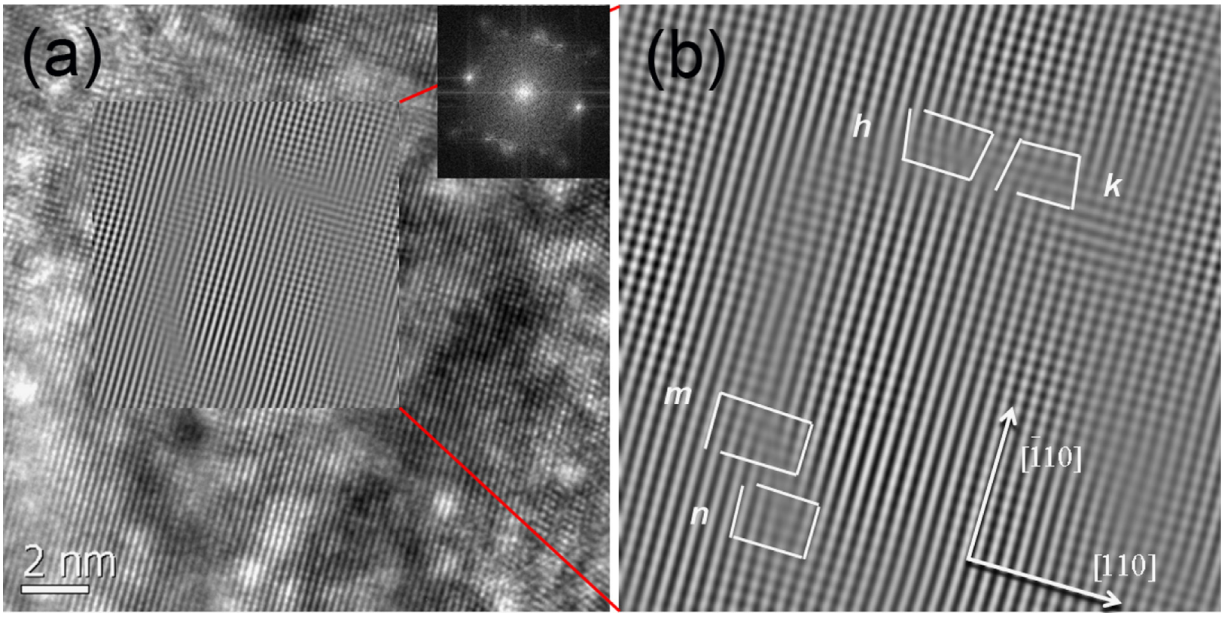

Fig. 2. (a) HRTEM image of NC Mo thin film; (b) enlarged view of (a).

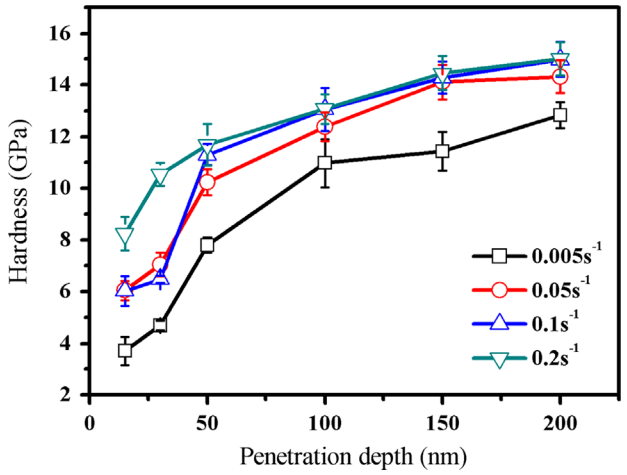

Fig. 3. Penetration depth dependence of the hardness of NC Mo thin film at selected loading strain rates.

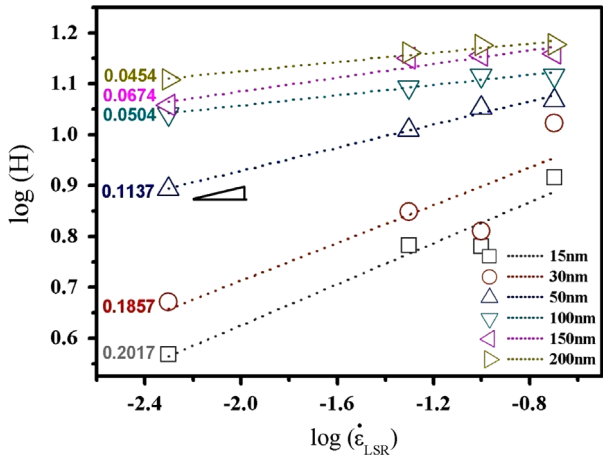

Fig. 4. Logarithmic plots of indentation hardness (H) as a function of loading strain rate ($\dot{\varepsilon}_{LSR}$) for NC-Mo; m was estimated from the slope of the linear fit.

loading regime, a dwell time of 100 s at each LSR was applied at the maximum load to evaluate the creep behavior of the Mo film. Depth control mode was conducted during indentation, and the prescript depths were set within a range of 15–200 nm, which was less than 1/7 thickness of the film to avoid substrate effects [8,9]. For each test, 12 indentations were carried out and at least 8 effective data were used for final analysis.

3. Results

Fig. 3 presented the dependence of hardness on penetration depth (h) and LSR for the NC Mo. For penetration depth dependence, significant inverse *indentation size effect* (ISE) was observed at all the LSRs applied. Take the data derived at LSR of 0.005 s^{-1} as an example: H decreased from ~12 GPa to 3.8 GPa as h was reduced from 200 nm to 15 nm. In general, at each penetration depth, positive strain rate sensitivities of the flow stress were obtained as the hardness increased with increasing LSR as shown in Fig. 3.

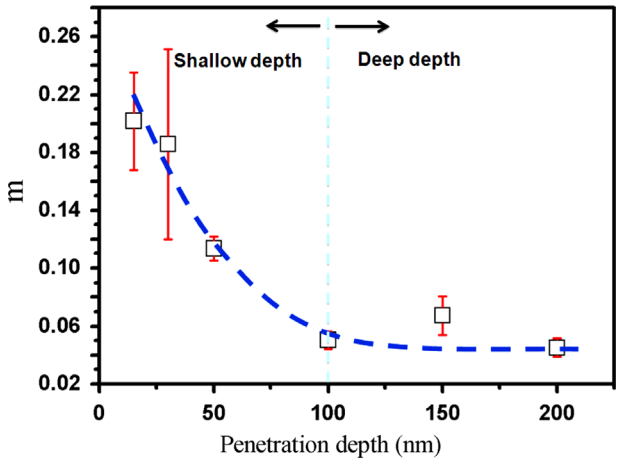

Fig. 5. Strain rate sensitivity of NC Mo thin film plotted as a function of penetration depth.

The strain rate sensitivities of flow stress m at various penetration depths were calculated from the double logarithmic curve of LSR and hardness as shown in Fig. 4. For instance, the value of m increased from 0.045 at 200 nm to 0.202 at 15 nm. The depth dependent m was summarized in the inset of Fig. 5, which indicated that m decreased from ~0.20 to a nearly stable value of ~0.04 when the penetration depth exceeded 100 nm.

4. Discussion

4.1. Inverse indentation size effect of hardness

In general, ISE could only be observed in coarse grained or single crystal metals [10,11]. For these materials, geometrically necessary dislocations (GNDs) restricted in a hemisphere with radius of indentation contact lengths were proposed to play a crucial role in increasing the hardness at shallower penetration depths [2]. Alternatively, dislocation mechanism related Taylor hardening model using kinetics and activation volume analysis were also used to interpret the ISE in aluminum and alpha brass [12–14]. In addition, it was also proposed that the tip roundness of indenter could affect the ISE behavior [15], as generated true GNDs pattern might be much denser than the idealized GNDs pattern predicted by Nix–Gao model [2]. Despite that, by observing the deformation induced lattice rotations of Cu via tress-dimensional electron backscattering diffraction, it has been indicated that the GND density could even decrease as hardness was enhanced at smaller indention depth corresponding to normal ISE behavior [16]. Despite the ISE behaviors related to the deformation mechanisms concerning GNDs, for NC or ultra-fine grained metals, however, there was generally no ISE because the restrictions came from high volume fraction of grain boundaries by interrupting the formation of GNDs. Therefore, the hardness of NC metals should be approximately a constant at various penetration depths.

Interestingly, despite the aforementioned ISE in coarse grained metals and nearly penetration depth independent hardness of NC metals, inverse ISE was observed in the present NC Mo at all the LSRs applied. As the grain size of the NC Mo was about 34.8 nm, GNDs could not operate in such tiny grains and hence should be ruled out in attributing the observed inverse ISE. Previously, inverse ISE was also observed in a number of single crystals [17] and coarse grained metals [18] via either micro-hardness or nanoindentation measurement. Obviously, the mechanisms proposed for the aforementioned inverse ISE behaviors could not explain the one observed in present NC Mo, as the aspects of both microstructural features [17,18] and deformation scales [17] are quite different from those for present NC Mo. Then, to identify the controlling mechanism(s) that dominates the inverse ISE in NC Mo, the penetration depth dependent m needs to be addressed, as discussed below.

4.2. Penetration depth dependent m

First of all, the hardness derived at the deeper penetration depth range of 100–200 nm should represent the intrinsic hardness of NC Mo, as surface effect could only affect its mechanical properties at a depth less than several tens of nanometers. It has been established that NC bcc metals exhibited much lower strain rate sensitivity than their coarse grained counterparts. Therefore, the values of m derived at the deeper penetration depth range shown in the inset of Fig. 5 were quite low, which were nonetheless consistent with the values reported previously for NC bcc metals.

Next, we try to interpret the dramatically increased m observed at the shallower penetration depth range (less than 100 nm). For bcc-Mo metal which critical temperature is 480 K, it was found that the edge components of dislocation lines moved more quickly than that of the screw parts at ambient temperature [5]. Moreover, the difference between the speeds of edge- and screw-components was proposed to be the controlling mechanism determining the magnitude of m in bcc metals. Specifically, the high strain rate sensitivity of coarse grained bcc metals relative to their NC counterparts was attributed to the slip of screw dislocations via the kink-pair nucleation mechanism, as the density of screw dislocations was reduced dramatically when the grain size decreased to nanoscale in bcc metals [6]. Despite that, the screw component within the high density mixed dislocations of Fig. 2 should influence the depth dependent m significantly if dislocation-mediated mechanism still dominated the plastic deformation of the present NC Mo film. Therefore, in the following, attributions from edge- and screw-components of mixed dislocations were used to interpret the depth dependent m.

The strain rate sensitivity of flow stress m may be obtained as [19]:

$$\frac{1}{m}=\frac{\partial \ln \dot{\gamma}}{\partial \ln \tau} \tag{1}$$

where τ is the shear stress and $\dot{\gamma}$ is the shear strain rate expressed by [6]:

$$\dot{\gamma}=b\rho v \tag{2}$$

Here, b is the magnitude of Burgers vector, ρ is the dislocation density and v is the dislocation speed. The strain rate of bcc metals could thence be written as:

$$\dot{\gamma}=b_e\rho_e v_e+b_s\rho_s v_s \tag{3}$$

where the subscripts e and s refer to edge dislocation and screw dislocation, respectively, while the other parameters have identical meanings as those of Eq. (2).

For bcc metals, as the grain size was reduced to nanoscale, the density of screw dislocations in Mo decreased dramatically whereas the densities of edge dislocations and mixed dislocations with edge- and screw-components increased [6]. For the present NC Mo, all the dislocations identified via TEM observation were mixed dislocations as shown in Fig. 2. Therefore, for the observed mixed dislocation in NC Mo, we redefined b_e and b_s in Eq. (3) to be the magnitude of Burgers vector of its edge- and screw-component, respectively. However, as screw dislocation in bcc metals moves much slower than edge dislocation, the edge-component in a mixed dislocation should also move much faster than the screw-component. Consequently, the strain rate sensitivity of flow stress m may be mainly caused by slip of the edge-component of mixed dislocations, namely:

$$\frac{1}{m}=\frac{\partial \ln \dot{\gamma}}{\partial \ln \tau}\approx\frac{\partial \ln b_e\rho_e v_e}{\partial \ln \tau} \tag{4}$$

This led to low strain rate sensitivity at the deeper penetration depth range, as the speed of edge dislocation v_e is much faster than that of screw dislocation in NC bcc metals [6].

As the penetration depth was reduced from 100 nm to 15 nm, surface effects were significantly enhanced as the deformation region underneath the indenter was approaching the free surface outside the vicinity of the residual indentation. There should be two surface effect related mechanisms, i.e., surface enhanced screw dislocation mobility and self-diffusion along indenter/sample interface, which may contribute to enhance the strain rate sensitivity of flow stress at the shallower penetration depth range (see inset of Fig. 5).

Consider first the mechanism of surface enhanced screw dislocation mobility. By compression testing of Ta, Mo and Fe micropillars, Kaufmann et al. [7] demonstrated that the screw dislocation mobility of bcc metals could be significantly enhanced

if free surface was very nearby. Typically, micrometer sized samples have very high surface to volume ratios. The pillars employed by Kaufmann et al. [7] had the shape of cuboid with three dimensions all larger than 1 μm. Apparently, the length scales of the cuboidal pillars were much larger than the penetration depth range selected in the present study. The surface enhanced screw dislocation mobility observed in cuboidal pillars should therefore be more significant in the deformed NC Mo at the shallow penetration depth range. As a result, contributions from the dislocation mobility of screw components to the strain rate sensitivity of flow stress should increase with decreasing penetration depth. Under these conditions, m can be approximated as:

$$\frac{1}{m}=\frac{\partial \ln \dot{\gamma}}{\partial \ln \tau}\approx\frac{\partial \ln b_s\rho_s v_s}{\partial \ln \tau} \tag{5}$$

Thus, within the nanoscale deformation range, the screw components may take over to carry out the plastic deformation, causing significantly enhanced m as the speed of screw dislocations in bcc metals is much slower than that of edge dislocations.

In addition to surface enhanced screw dislocation mobility, another surface effect may also attribute the enhanced m as the penetration depth was reduced. In nanoscale creep deformation of both crystalline metals [20,21] and amorphous metals [22], it has been found that interfacial diffusion between the indenter and the sample was the dominant mechanism if the penetration depth was smaller than tens of nanometers. These studies indicated further that the interfacial diffusion mechanism was insensitive to microstructure and the strain rate sensitivity exhibited strong dependence on indentation size as the indenter approached free surface. For the present NC Mo thin film deformed at an indentation depth less than 100 nm, the aforementioned interfacial diffusion process could also operate and attribute the enhanced m. Given that the value of m shown in the inset of Fig. 5 reached as high as ~0.2, the mechanism of interfacial diffusion should dominate plastic deformation at the penetration depth of 15 nm, as the value of m corresponding to dislocation-mediated mechanism was generally smaller than 0.06 for bcc metals [10].

The enhanced strain rate sensitivity of flow stress at the shallower penetration depth range may be contributed by both of the two surface effects discussed above, as we cannot rule out any of them based on the present analysis.

4.3. Surface effects induced inverse ISE

Based on the two surface effects discussed in the previous section, we readdress the issue of inverse ISE as observed in Fig. 3. At sufficiently deep penetration depths, the screw dislocations/components involved in plastic deformation should exhibit low mobility, leading to high indentation hardness. As the penetration depth was reduced, the mobility of screw dislocations/components increased by approaching the free surface, thus causing the indentation hardness to decrease. On the other hand, dislocation pile-up would easily occur at deep penetration depths as the deformed region is restricted by surrounding un-deformed regions and grain boundaries. The back stress generated from dislocation pile-up also contributes to increase the indentation hardness. In contrast, at shallow penetration depths, dislocations would escape more easily from the free surface nearby. Specifically, the minimum penetration depth (15 nm) adopted in the present study was much smaller than the average grain size of NC Mo. Therefore, the lowest indentation hardness was achieved at the depth of 15 nm because, at such deformation scale, dislocations may escape even without the restriction of grain boundaries.

In addition to surface effect on dislocation mobility, interfacial diffusion could also affect indentation hardness at shallow penetration depths. It is well known that the activation energy for self-diffusion along free surface is much lower than that required for all other mechanisms such as dislocation intersection, lattice diffusion, pipeline diffusion, and grain boundary diffusion/sliding. Therefore, when the deformed region underneath the indenter was very near the free surface, the interface between the indenter and the specimen is the easiest way for mass transfer because no physical or chemical bonds existed at the interface. Correspondingly, the indentation hardness decreased.

5. Conclusion

By systematically changing the penetration depth and loading strain rate (LSR), the hardness and strain rate sensitivity of NC bcc Mo thin film were investigated under nanoindentation testing. It was found that, at all the LSRs applied, indentation hardness decreased dramatically with decreasing penetration depth. To the authors' best knowledge, this is the first report that the hardness of NC metals (including fcc and bcc lattice structures) exhibited inverse indentation size effect. The hardness of NC Mo was also found to exhibit depth dependent strain rate sensitivity, with the maximum value of m reaching as high as ~0.2. It was proposed that surface effects altering the mobility of screw component in mixed dislocations along with the path length of interfacial diffusion were the dominant mechanisms underlying the observed size effects in NC Mo.

Acknowledgments

This work was supported by the National Basic Research Program of China (2011CB610306), the National Natural Science Foundation of China (51271141, 51171141), Program for New Century Excellent Talents in University (NCET-11–0431).

References

[1] G.I. Taylor, Proc. R. Soc. Lond. 145 (1934) 362–387.
[2] W.D. Nix, H. Gao, J. Mech. Phys. Solids 46 (1998) 411–425.
[3] H. Li, R.C. Bradt, J. Non-Crys. Solids 146 (1992) 197–212.
[4] I. Manika, J. Maniks, Acta Mater. 54 (2006) 2049–2056.
[5] A. Schneider, D. Kaufmann, B. Clark, C. Frick, P. Gruber, R. Mönig, O. Kraft, E. Arzt, Phys. Rev. Lett. 103 (2009) 105501.
[6] G.M. Cheng, W.W. Jian, W.Z. Xu, H. Yuan, P.C. Millett, Y.T. Zhu, Mater. Res. Lett. 1 (2013) 26–31.
[7] D. Kaufmann, A.S. Schneider, R. Mönig, C.A. Volkert, O. Kraft, Int. J. Plast. 49 (2013) 145–151.
[8] D. Faghihi, G.Z. Voyiadjis, Mech. Mater. 44 (2012) 189–211.
[9] R. Saha, W.D. Nix, Acta Mater. 50 (2002) 23–38.
[10] N.A. Stelmashenko, M.G. Wall, L.M. Brown, Y.V. Milman, Acta Metall. Mater. 41 (1993) 2855–2865.
[11] A. Gouldstone, N. Chollacoop, M. Dao, J. Li, A. Minor, Y. Shen, Acta Mater. 55 (2007) 4015–4039.
[12] A.A. Elmustafa, D.S. Stone, Mater. Sci. Eng. A358 (2003) 1–8.
[13] A.A. Elmustafa, D.S. Stone, J. Mech. Phys. Solids 51 (2003) 357–381.
[14] A.A. Elmustafa, D.S. Stone, Indentation size effect in polycrystalline F.C.C. metals, Acta Mater. 50 (2002) 3641–3650.
[15] J. Alkorta, J.M. Martinez-Esnaola, J.G. Sevillano, Acta Mater. 54 (2006) 3445–3452.
[16] E. Demir, D. Raabe, N. Zaafarani, S. Zaefferer, Acta Mater. 57 (2009) 559–569.
[17] K. Sangwal, Mater. Chem. Phys. 63 (2000) 145–152.
[18] G.Z. Voyiadjis, A.H. Almasri, T. Park, Mech. Res. Commun. 37 (2010) 307–314.
[19] Q. Wei, S. Cheng, K.T. Ramesh, E. Ma, Mater. Sci. Eng. A381 (2004) 71–79.
[20] F. Wang, P. Huang, T.J. Lu, J. Mater. Res. 24 (2011) 3277–3285.
[21] F. Wang, P. Huang, K.W. Xu, Appl. Phys. Lett. 90 (2007) 161921.
[22] F. Wang, J.M. Li, P. Huang, W.L. Wang, T.J. Lu, K.W. Xu, Intermetallics 38 (2013) 156–160.